A thermodynamic framework for a system with itinerant-electron magnetism

A thermodynamic framework for a system with itinerant-electron magnetism

Y Wang[1], L G Hector Jr[2], H Zhang[1], S L Shang[1], L Q Chen[1] and Z K Liu[1]

[1] Materials Science and Engineering, The Pennsylvania State University, University Park, PA 16802, USA
[2] GM R&D Center, 30500 Mound Road, Warren, MI 48090, USA

Abstract
Thermodynamic fluctuation among many electronic states in systems with 'itinerant-electron' magnetism is addressed with a first-principles formulation of the Helmholtz energy. The Ce $\gamma-\alpha$ phase transition is used as an illustrative case. The $k_B \ln(2J + 1)$ form for the magnetic entropy that is commonly found in the literature is replaced with an expression that is derived from configurational fluctuations among nonmagnetic, ferromagnetic, and antiferromagnetic electronic states. Predicted first- and second-order magnetic phase transitions are in close accord with experiment. The mixture of states leads to a Schottky anomaly in the Ce specific heat.

(Some figures in this article are in colour only in the electronic version)

1. Introduction

Since the discovery of the electron spin, the role of spin freedom has been the focus of the theory of magnetism. Of particular interest is 'itinerant-electron' magnetism [1, 2] which leads to intriguing properties such as the well-documented ferromagnetic–paramagnetic transition. Some superconducting compounds exhibit 'itinerant-electron' magnetism. Examples are the cuprates [3], the newly-discovered iron pnictides [4], and heavy-fermion compounds [5], which exhibit the antiferromagnetism $\rightarrow$ spin glass $\rightarrow$ superconductor phase transition sequence and specific heat anomalies. 'Itinerant-electron' magnetism is also operative in multiferroics [6] and lithium transition metal phosphates for rechargeable batteries [7] for which ferroelectric, ferro/antiferromagnetic, and ferroelastic phases coexist.

We recently developed a thermodynamic framework for f-electron systems with 'local-moment' mechanism [8]. We applied our framework to the Ce $\gamma-\alpha$ isostructural phase transition (as a representative case) assuming only two Ce states, i.e. low-volume, nonmagnetic and high-volume ferromagnetic. While our predictions of the critical point and equation of state were reasonable, our model overestimated the entropy change of the transition along the phase boundary. We believe that this disparity is due to the adopted 'local-moment' mechanism. This can be demonstrated through analysis of the total entropy change $\Delta S = \Delta S_f + \Delta S_{lat} + \Delta S_{el}$ along the $T-P$ phase boundary where ΔS_f, ΔS_{lat}, ΔS_{el} are the magnetic contribution, the lattice contribution, and electronic contributions due to thermal electronic excitation within the same magnetic configuration, respectively. Using the Clapeyron equation, $\Delta S = \Delta V \, dP/dT$, Allen and Liu [9] estimated $\Delta S \sim 1.54k_B$ (k_B is the Boltzmann constant) which falls within the 1.4–$1.6k_B$ range from experiments [10, 11]. Jeong *et al* [12] measured $0.75 \pm 0.15k_B$ for ΔS_{lat}. ΔS_{el} is small and can be neglected. Taking away the lattice contribution, the experimental ΔS_f then falls in the 0.5–$1.0k_B$ range, suggesting 'itinerant-electron' magnetism in the Ce $\gamma-\alpha$ transition. Theoretically, 'local-moment' magnetism results (at a sufficiently high temperature) in $\Delta S_f = k_B \ln(2J + 1)$ (Ce can be viewed as having just one electron that contributes to the magnetic entropy per atom) where $J = L \pm X$ is the local total angular momentum ($L = 3$ is the orbital momentum of an f-electron and $X = 1/2$ is the electron spin angular momentum). Numerically, Johansson *et al* [13] (following the Mott transition (MT) model), Allen and Liu [9] (following the Kondo volume collapse (KVC) model), and Lipp *et al* [14] (following the KVC model) employed $J = 2.5$, leading to $\Delta S_f = 1.79k_B$ ($k_B \ln 6$). Lüders *et al* [15] employed $J = 3.5$, leading to $\Delta S_f = 2.08k_B$ ($k_B \ln 8$). These values are all well outside of the 0.5–$1.0k_B$ experimental range estimated above. If one assumes 'itinerant-electron' magnetism by which

an f-electron is limited to having only spin up, spin down, and spin zero (nonmagnetic) states (at a sufficiently high temperature), then $\Delta S_f = 1.10 k_B$ ($k_B \ln 3$). Alternatively, $\Delta S_f = 0.69 k_B$ ($k_B \ln 2$) if an f-electron is limited to having only spin up and spin down states.

In the present paper, we reformulate our previous 'local-moment' mechanism framework [8] in terms of 'itinerant-electron' magnetism. Our new framework, which is based upon a fundamental partition function, is detailed in section 2 along with the associated Helmholtz free energy, thermal population, magnetic entropy, and magnetic specific heat. In section 3, we discuss the physics associated with the thermodynamic formulation in section 2. Section 4 is the computational detail for an investigation of the well-known Ce γ–α isostructural phase transition which is used as a prototype system to demonstrate our new framework. A discussion of our results in terms of the 0 K energetics, the temperature evolution of the double wells (tangents) along the free energy isotherm, the thermal population, the specific heat anomaly, and comparison with the Kondo–Anderson model are provided in section 5. The main developments in the paper are summarized in section 6.

2. Thermodynamic framework

We consider a magnetic lattice with N atoms where volume V and temperature T are constant. For such a system, the partition function, Z, is written as [16]:

$$Z = \sum_{\sigma} w^{\sigma} \sum_{i \in \sigma, \rho \in \sigma} \exp[-\beta \varepsilon_i(N, V, \rho)]. \quad (1)$$

Here, σ identifies the electronic states, each distinguished by different spin orientation distributions in the lattice sites at which the local spin can be up, down, and zero (zero means a locally nonmagnetic site in the present theory). In addition, $\beta = 1/k_B T$, w^{σ} is the multiplicity of electronic state σ, i represents the vibrational states belonging to the electronic state σ, ρ labels the electronic distributions associated with electronic state σ, and $\varepsilon_i(N, V, \rho)$ is the energy eigenvalue of the corresponding microscopic Hamiltonian. Summation over all states belonging to a specific electronic state σ gives

$$\sum_{i \in \sigma, \rho \in \sigma} \exp[-\beta \varepsilon_i(N, V, \rho)] = Z^{\sigma} = \exp[-\beta F^{\sigma}(N, V, T)]. \quad (2)$$

It is immediately apparent that $F^{\sigma}(N, V, T)$ is the Helmholtz free energy of electronic state σ, and the thermal population of electronic state σ is thus:

$$x^{\sigma} = w^{\sigma} Z^{\sigma}/Z. \quad (3)$$

We emphasize here that the multiplicity w^{σ} in equations (1) and (3) means that the system has a total of w^{σ} electronic states that are equivalent to electronic state σ by space and spin symmetry. Furthermore, with $F = -k_B T \ln Z$ [16], we find the Helmholtz free energy for a system with N atoms to be

$$F(N, V, T) = \sum_{\sigma} x^{\sigma} F^{\sigma}(N, V, T) - T S_f(N, V, T), \quad (4)$$

where an important ancillary result is the magnetic entropy

$$S_f(N, V, T) = -k_B \sum_{\sigma} x^{\sigma} \ln(x^{\sigma}/w^{\sigma}). \quad (5)$$

We then find the total entropy is

$$S(N, V, T) = S_f(N, V, T) + \sum_{\sigma} x^{\sigma} S^{\sigma}(N, V, T), \quad (6)$$

where $S^{\sigma} = -(\partial F^{\sigma}/\partial T)_V$ is the entropy of electronic state σ. Furthermore, we deduce the specific heat at constant volume from $C_V = (\partial(F + TS)/\partial T)_V$ and the result is

$$C_V(N, V, T) = C_f(N, V, T) + \sum_{\sigma} x^{\sigma} C_V^{\sigma}(N, V, T). \quad (7)$$

Note that C_V^{σ} in equation (7) is the specific heat of electronic state σ. The magnetic specific heat due to the configurational coupling or spin fluctuation is thus

$$\begin{aligned} C_f(N, V, T) = \frac{1}{k_B T^2} &\left\{ \sum_{\sigma} x^{\sigma} [E^{\sigma}(N, V, T)]^2 \right. \\ &\left. - \left[\sum_{\sigma} x^{\sigma} E^{\sigma}(N, V, T) \right]^2 \right\}, \end{aligned} \quad (8)$$

with the internal energy given by $E^{\sigma} = F^{\sigma} + T S^{\sigma}$ and the entropy of electronic state σ given by $S^{\sigma} = -(\partial F^{\sigma}/\partial T)_V$.

3. Physics

3.1. Ergodicity

The thermodynamic framework detailed in section 2 satisfies the condition of ergodicity in statistical physics [16]. Therefore, equation (3) links the total Helmholtz free energy of the system and the Helmholtz free energy of an individual electronic state. The thermodynamics is complete as described by equations (3)–(8). Moreover, if there are s magnetic electronic states at each lattice site, the summation over σ in equations (1) and (4) will contain s^N terms. Note that the summation over σ is in addition to the summation over the local lattice vibrations and the local thermal electronic excitation which have been accounted in $F^{\sigma}(N, V, T)$—the Helmholtz free energy of electronic state σ.

3.2. Driving force for the magnetic phase transition

We note that it is the multiplicity, w^{σ}, that controls the magnitude of x^{σ} in equation (3) and therefore the magnetic phase transition. This can easily be understood through the following observations. If w^{σ} is merged into the exponential part in equation (1), then an extra entropy contribution of $k_B T \ln w^{\sigma}$ is added to the free energy $F^{\sigma}(N, V, T)$ (equation (4)) of the individual electronic state σ. As a result of the differences in w^{σ}, the energy barrier due to the 0 K energy difference between different electronic states can be overcome by this entropy with increasing temperature. This renders the free energies of some of the 0 K metastable electronic states lower than that of the original 0 K ground state, resulting in the magnetic phase transition. We believe that this is the underlying physics associated with the Ce γ–α

transition (nonmagnetic-paramagnetic), the well-documented ferromagnetic–paramagnetic transition [17], and the spin-density-wave to paramagnetic transition in the new iron-based superconductor family (discovered following the seminal work of Kamihara *et al* [4]).

3.3. Schottky anomaly

Equation (8) is a generalization of the Schottky specific heat anomaly for a two-state system [17]. As we shall demonstrate, this implies that the specific heat has a peak value at a specific temperature at the point of the magnetic phase transition.

4. Computational details

To illustrate our theory, we again investigate thermodynamics of the Ce γ–α transition [14] which continues to be the subject of extensive study. In fact, debates persist regarding the suitability of the Mott transition (MT) model [13, 15, 18] and the Kondo volume collapse (KVC) model [9, 19, 20].

We treat Ce as a system having $N = 2$ magnetic lattice sites at each of which the atom can be both magnetic (with spin either up or down) and nonmagnetic (for simplicity, we will use 'spin zero' to label the nonmagnetic state); this makes up $3^N = 9$ spin distributions (electronic states). However, calculations demonstrate that the mixed space combination of spin zero and spin up (down) is not numerically stable. Convergence to either nonmagnetic or ferromagnetic states always occurs. Combinations of spin zero and spin up (down) have an associated multiplicity of 4, i.e., 01, 0$\bar{1}$, 10, and $\bar{1}$0, where 0, 1, and $\bar{1}$ represent spin zero, up, and down, respectively. We assume that these combinations are each high in energy and hence can be neglected. The remaining electronic states are nonmagnetic (00), antiferromagnetic (1$\bar{1}$ = $\bar{1}$1, body-centered tetragonal [21] with c/a = 1.4142) and ferromagnetic (11 = $\bar{1}\bar{1}$) with multiplicities of 1, 2, and 2, respectively. We note that the present theory can readily address a larger (e.g. $N > 2$) system and expect some improvement in the major results (e.g. ΔS_f) relative to experimental measurements through inclusion of additional states. However, inclusion of additional states is unwarranted here since our focus on only the nonmagnetic, antiferromagnetic, and ferromagnetic states is sufficient for demonstrating that the theory accurately addresses itinerant-electron magnetism. This can be understood by the fact that for arbitrary N, the number of states of the system is 3^N which gives rise to, at high enough temperature, an entropy of $Nk_B \ln 3$ for the N site system, i.e., $k_B \ln 3$ per site-N-independent at high enough temperature.

We calculate $F^\sigma(N, V, T)$ using [16]

$$F^\sigma(N, V, T) = E_c^\sigma(N, V) + F_{lat}^\sigma(N, V, T) + F_{el}^\sigma(N, V, T). \quad (9)$$

Note that E_c^σ is the 0 K static total energy, F_{lat}^σ is the lattice vibrational free energy, and F_{el}^σ is the thermal electronic free energy.

The 0 K static total energy in equation (9) is calculated with the Dudarev DFT + U method [22] in VASP [23] with spin polarization as in the previous work [8].

The direct method to lattice dynamics can be used (see our previous model [8]) to estimate the free energy due to lattice vibrations in the present thermodynamic formulation. However, extensive phonon calculations revealed imaginary modes in the magnetic structures with lower atomic volumes (<32 Å^3). Previously [8], we employed extrapolation to get the lattice contributions to the free energy. However, in this work, we find that similar extrapolation results in non-negligible uncertainty for the antiferromagnetic state since its energy is too close to the nonmagnetic state (the extrapolation for the ferromagnetic state works well due to its relatively large energy difference with the nonmagnetic state). We therefore adopt the Debye–Grüneisen approach [24, 25] which requires only the total energy with volume as input. The Debye–Grüneisen approach does not change the main physics of the present work. In fact, it has been frequently employed in the literature [14] to compute free energies due to lattice vibrations without appeal to lattice dynamic calculations. Furthermore, the Debye–Grüneisen approach is a suitable alternative to more computationally demanding phonon calculations or in situations where phonon calculations reveal imaginary modes or the system size precludes first-principles calculations altogether. We calculated the Debye temperature using $\theta_D^\sigma = 154.79[(V/N)^{1/3} B^\sigma(V)/M]^{1/2}$ [24, 25] where B^σ is the 0 K single crystal bulk modulus (GPa) and M is the average atomic mass (amu), and V is the average atomic volume (Å^3). Here, the prefactor of 154.79 differs from that of Moruzzi *et al* [24] by a factor of 1.086. The thermal averages of our calculated Debye temperatures are 145 K for α-Ce and 104 K for γ-Ce. These are in reasonably close accord with the experimentally estimated values of 134 K for α-Ce and 104 K for γ-Ce from Jeong *et al* [12]. For Debye temperature values versus pressure, the ultrasonic measurements of Voronov *et al* [26] gave ~148 K for the alpha phase and 136 K for the gamma phase at the transition.

The remaining term in equation (9), F_{el}^σ, was determined via integration over the electronic DOS following the Fermi–Dirac distribution [8, 21, 27].

5. Results and discussion

5.1. Evolution of double wells along the free energy isotherm

Figure 1(a) shows our computed 0 K static total energies with atomic volume for the nonmagnetic (NM), antiferromagnetic (AFM), and ferromagnetic (FM) Ce states. The equilibrium volume energies reveal that the NM state is the lowest of the three states. However, the AFM state is intermediate in energy to the NM and FM states since the energy at its equilibrium volume is just above that of the NM state but substantially lower than that of the FM state. Figure 1(b) shows our computed free energy isotherms. The γ–α phase transition in Ce is noted by the double tangents which merge at our predicted critical point values of T_c = 546 K and P_c = 2.05 GPa. This is in close accord with the experimental values of 600 K and 2.0 GPa reviewed by Koskenmaki and Gschneidner [28]. In comparison, the critical points measured from other experiments are: 1.5 GPa and 480 K [14]; 1.8 GPa
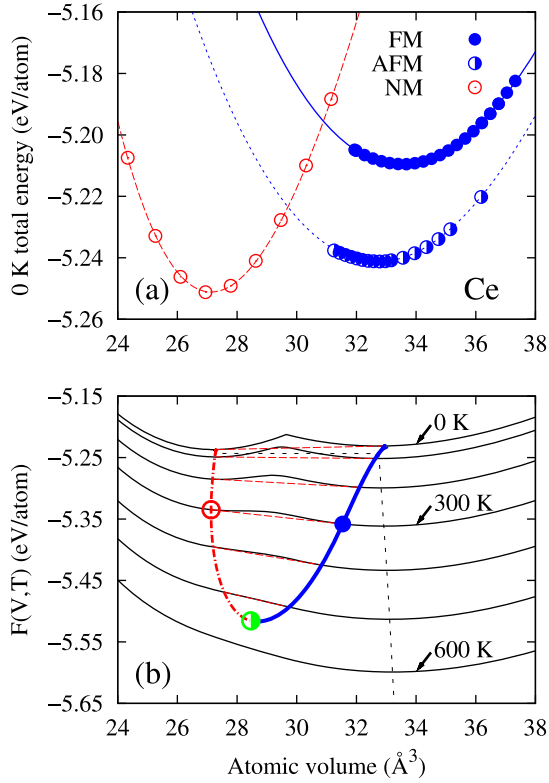
Figure 1. (a) dot–dashed line with ○ (red), dashed line ◑ (blue), and solid line with ● (blue) represent the 0 K static total energies for nonmagnetic, antiferromagnetic, and ferromagnetic electronic states of Ce, respectively. (b) The solid lines denote $F(N, V, T)$ (per atom) from 0 to 600 K at $\Delta T = 100$ K; the heavy dot–dashed (α-Ce, red) and solid (γ-Ce, blue) looping curves enclose the two-phase region with the light red dot–dashed lines connecting the common tangents of each isotherm; the black dashed line denotes the zero pressure equilibrium state at given T; ○ (red) and ● (blue) emphasize the phase boundary at 300 K while ◑ (green) is the critical point.

and 485 K [11]; 1.45 GPa and 480 K [29]; 1.75 GPa and 550 K [30].

5.2. T–V and T–P phase diagrams

Based on the free energy dependency of T and V, we have also calculated the Ce phase diagram in the T–V and T–P planes. Comparisons with experimental data [10–12, 14, 28–33] are shown in figures 2(a) and (b), respectively. Two results from Lipp *et al* [14] based upon the KVC model fitting are also plotted in figure 2(b) for comparison. Our theory predicts that the critical point for the Ce γ–α transition is actually a tri-critical point below which is a two-phase region (yellow shadow in figure 2(a) of the T–V phase diagram) composed of nonmagnetic, antiferromagnetic, and ferromagnetic states, and above which the transition is second or higher order. The magnetic entropy S_{f} due to configurational coupling plays a crucial role in our prediction of the tri-critical point. Without S_{f}, the transition is always first order over 0–800 K. Figure 2(a) also shows a tentative phase boundary which is determined by finding the volume point that gives a 50% thermal population of the nonmagnetic state.
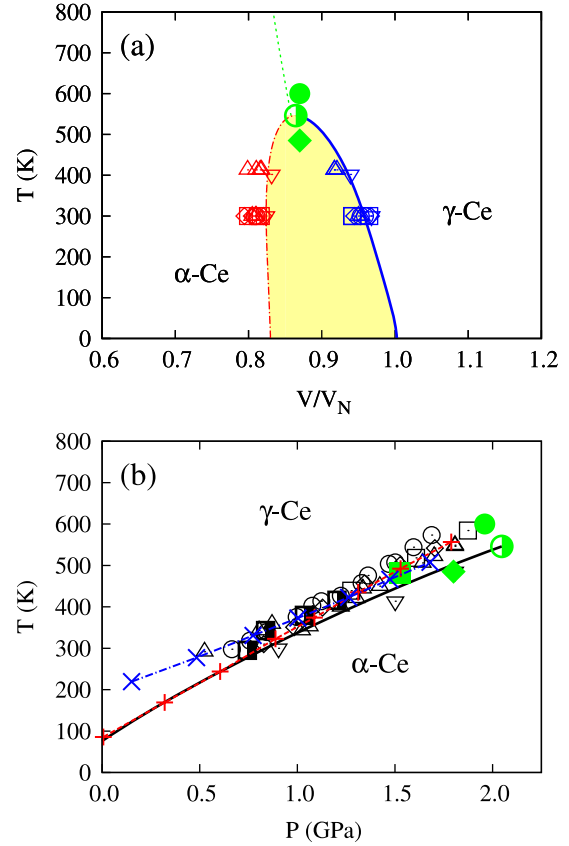

Figure 2. (a) V_N denotes the atomic volume at 300 K and 0 GPa. The dot–dashed (red) and solid (blue) looping branches denote α-Ce and γ-Ce, respectively. ◑ (green) represents the predicted critical point (T_{c}) from the present work; the dashed (green) line denotes a tentative phase boundary above T_{c}; the experimental data are due to Schiwek *et al* [11] (red △ and blue △); [12] (red ○ and blue ○); [33] (red □ and blue □); [32] (red ◇ and blue ◇); [10] (red ▽ and blue ▽); [11] (green ◆); and [28] (green ●). (b) The solid (black, overlapped with the red dashed line at low P) line represents the phase boundary predicted in the present work. The experimental phase boundary is due to Jayaraman [30] (black ◇); Schiwek *et al* [11] (black ▽); Poniatovskii [31] (black △); [14] (black ◧); [10] (black ○); and [29] (black □). Big green ■ represents the recently measured critical point by Lipp *et al* [14]. The red dashed (with the + sign) and blue dot–dashed (with the × sign) lines represent two KVC model fittings by Lipp *et al* [14].

5.3. Entropy changes along the phase boundary

Next, we discuss the entropy change associated with the Ce γ–α phase transition in terms of magnetism and lattice vibration. Figure 3(a) shows predicted components of the total entropy change. At 300 K we predict $\Delta S = 1.40 k_{\mathrm{B}}/$atom (with $\Delta S_{\mathrm{lat}} = 0.94 k_{\mathrm{B}}/$atom). Our theory, therefore, in the form of itinerant magnetism, agrees well with available experimental data. Figure 3(b) shows the individual contribution to the free energy change along the phase boundary in terms of $T\Delta S$, ΔE, and $P\Delta V$. Close agreement is noted for each thermodynamic term between the present theory and the experiments [10, 11].

5.4. Temperature evolution of the thermal population

Near the critical point, our theory predicts that the system is a mixture of the various electronic states. Figure 4(a) depicts
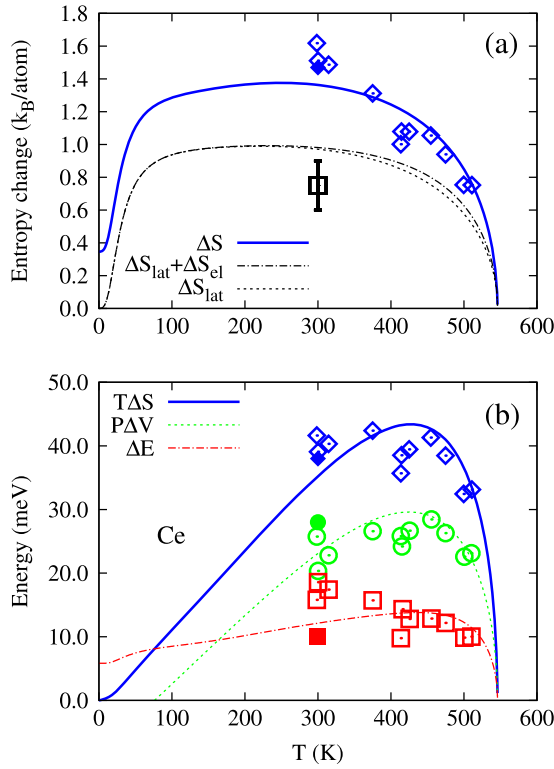
Figure 3. (a) The calculated entropy changes in terms of lattice vibration only (black dashed line), lattice vibration plus thermal electron (black dot–dashed line), and lattice vibration plus thermal electron and plus configuration coupling (solid blue). Black □ (with error bars) from Jeong *et al* [12] is their estimated vibrational entropy change at 0.7 GPa of γ-Ce relative to α-Ce. Other open (solid) symbols are from the measurements of Schiwek *et al* [11] [10].(b) The measured data by Schiwek *et al* [11] and Beecroft and Swenson [10] plotted in the form of $T\Delta S$ (blue diamonds), ΔE (green circles), and $P\Delta V$ (red squares) along the γ–α phase boundary. The curves are from the present calculations.
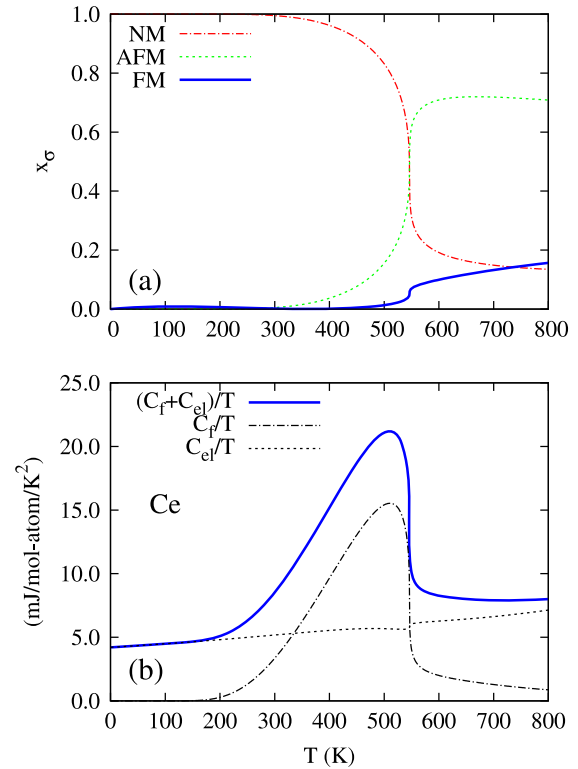
Figure 4. (a) Thermal populations of the nonmagnetic (red dot–dashed), antiferromagnetic (green dashed), and ferromagnetic (blue solid) as a function of temperature at the critical pressure of 2.05 GPa. (b) C_{el}/T, (black dashed line), C_f/T (black dot–dashed line), and their sum $(C_f + C_{el})/T$ (blue solid line) at 2.05 GPa.

calculated thermal populations (x^σs) of the nonmagnetic, antiferromagnetic, and ferromagnetic electronic states at the 2.05 GPa critical pressure. For $T < 300$ K, the system consists mainly of the nonmagnetic Ce state which results in α-Ce. For $T > 300$ K, the thermal populations of the magnetic states increase with increasing temperature. Finally, for $T > 546$ K (the critical point), 70% of the system is composed of the antiferromagnetic Ce state with the remaining 30% consisting of the nonmagnetic and ferromagnetic Ce states. This is in agreement with the experimental observations [28, 34, 35] that γ-Ce is magnetic with a partially disordered local-moment (paramagnetic) and that α-Ce is nonmagnetic.

5.5. Schottky anomaly

The mixture of Ce states further results in the specific heat anomaly [36, 37] which is a characteristic of critical phenomena in many materials. For superconductors, the specific heat anomaly is usually explained in terms of the pseudogap or electron–phonon interaction [38, 39].

Figure 4(b) shows our predicted temperature evolution of C_f/T, C_{el}/T (C_{el} is the electronic specific heat), and

their sum, at our predicted 2.05 GPa critical pressure. Our theory suggests the following: (a) below $\sim$500 K, $(C_f + C_{el})/T$ shows an exponential temperature dependence due to the thermodynamic fluctuation among the nonmagnetic, ferromagnetic, and antiferromagnetic states; (b) a peak appears at $\sim$500 K in the $(C_f + C_{el})/T$ curve, which typically suggests the Schottky anomaly; (c) the electronic specific heat coefficient (C_{el}/T) is linear against T; (d) above $\sim$500 K the sum of C_f/T and C_{el}/T renders $(C_f + C_{el})/T$ temperature-independent. For the total specific heat, our calculated specific heat at 300 K and 2.05 GPa is $\sim$28 J/mole atom compared with the measured value of $\sim$31 J/mole atom at 300 K and 2.0 GPa by Bastidet *et al* [36]. We note that at 360 K and 2.05 GPa, our calculated specific heat is $\sim$31 J/mole atom.

5.6. Comparison with the Kondo–Anderson model

We use figure 5 to summarize the underlying physics of the 'itinerant-electron' magnetism model. The present model closely resembles the magnetic impurity model of Anderson [9] associated with the Kondo effect [1, 40–42] for a lattice of magnetic impurities. The physical essence of the Kondo effect is the role of spin of the magnetic impurity as a function of temperature. Kouwenhoven and Glazman [41] presented a cogent summary of the physics of the Anderson model. The electrons from the magnetic impurity, which have a spin of 1/2 and z-component fixed as either 'spin up' or 'spin
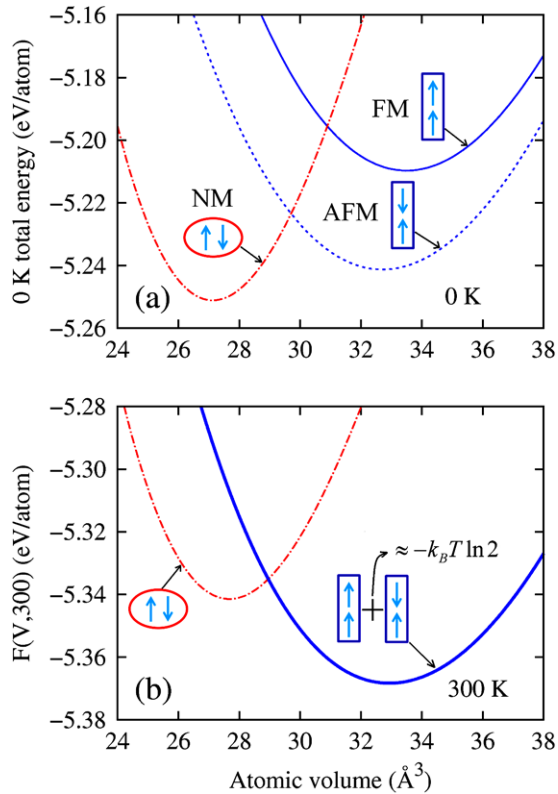
Figure 5. Comparison with the Kondo–Anderson model. (a) 0 K static energy; (b) 300 K free energy.

down', coexist with the mobile electrons (a Fermi sea) in the host metal. According to Kouwenhoven and Glazman [41] '···all the states with energies below the so-called Fermi level are occupied, while the higher-energy states are empty. However, so-called exchange processes can take place that effectively flip the spin of the impurity from spin up to spin down, or vice versa, while simultaneously creating a spin excitation in the Fermi sea'. In other words [1, 40], at low temperature, the impurity magnetic moment and one conduction electron moment bind very strongly to form an overall nonmagnetic state where, at high temperatures, the binding is broken resulting in a magnetic entropy of approximately $k_B \ln 2$.

As illustrated in figure 5, our itinerant-magnetism model for the Ce transition assumes that there are two groups of electronic states, namely, the nonmagnetic group (just one state) and the magnetic group formed by the ferromagnetic and antiferromagnetic states. At 0 K equilibrium, the nonmagnetic is the occupied ground state and the magnetic states are empty. At increasing temperature, being slightly different from the Anderson model, our model has the magnetic entropy term in equation (5). Taking the simplest case where the system is limited to magnetic states, at high enough temperature the mixture between the ferromagnetic and antiferromagnetic states results in a magnetic entropy of $\sim k_B \ln 2$. It is the entropy that controls the Ce γ–α phase transition. We find that the lattice contribution and magnetic contribution to Ce γ–α phase transition are of the same magnitude.

6. Conclusions

In summary, we have developed a first-principles thermodynamic framework for materials that exhibit 'itinerant-electron' magnetism. Using Ce as an illustrative example, we have quantitatively addressed the mixing of nonmagnetic, antiferromagnetic, and ferromagnetic 4f-states at finite temperatures. The present theoretical formulation is applicable to a whole host of technologically relevant materials.

Acknowledgments

References

[1] Yang Y F, Fisk Z, Lee H O, Thompson J D and Pines D 2008 *Nature* **454** 611
[2] Saxena S S, Agarwal P, Ahilan K, Grosche F M, Haselwimmer R K W, Steiner M J, Pugh E, Walker I R, Julian S R, Monthoux P, Lonzarich G G, Huxley A, Sheikin I, Braithwaite D and Flouquet J 2000 *Nature* **406** 587
[3] Zhang S C 1997 *Science* **275** 1089
[4] Kamihara Y, Watanabe T, Hirano M and Hosono H 2008 *J. Am. Chem. Soc.* **130** 3296
[5] Park T, Ronning F, Yuan H Q, Salamon M B, Movshovich R, Sarrao J L and Thompson J D 2006 *Nature* **440** 65
[6] Zhao T, Scholl A, Zavaliche F, Lee K, Barry M, Doran A, Cruz M P, Chu Y H, Ederer C, Spaldin N A, Das R R, Kim D M, Baek S H, Eom C B and Ramesh R 2006 *Nat. Mater.* **5** 823
[7] Van Aken B B, Rivera J P, Schmid H and Fiebig M 2007 *Nature* **449** 702
[8] Wang Y, Hector L G Jr, Zhang H, Shang S L, Chen L Q and Liu Z K 2008 *Phys. Rev.* B **78** 104113
[9] Allen J W and Liu L Z 1992 *Phys. Rev.* B **46** 5047
[10] Beecroft R I and Swenson C A 1960 *J. Phys. Chem. Solids* **15** 234
[11] Schiwek A, Porsch F and Holzapfel W B 2002 *High Pressure Res.* **22** 407
[12] Jeong I K, Darling T W, Graf M J, Proffen T, Heffner R H, Lee Y, Vogt T and Jorgensen J D 2004 *Phys. Rev. Lett.* **92** 105702
[13] Johansson B, Abrikosov I A, Alden M, Ruban A V and Skriver H L 1995 *Phys. Rev. Lett.* **74** 2335
[14] Lipp M J, Jackson D, Cynn H, Aracne C, Evans W J and McMahan A K 2008 *Phys. Rev. Lett.* **101** 165703
[15] Lüders M, Ernst A, Dane M, Szotek Z, Svane A, Kodderitzsch D, Hergert W, Gyorffy B L and Temmerman W M 2005 *Phys. Rev.* B **71** 205109

[16] Landau L D and Lifshitz E M 1980–1981 *Statistical Physics* (Oxford: Pergamon)
[17] Kittel C 2005 *Introduction to Solid State Physics* (Hoboken, NJ: Wiley)
[18] Johansson B 1974 *Phil. Mag.* **30** 469
[19] Amadon B, Biermann S, Georges A and Aryasetiawan F 2006 *Phys. Rev. Lett.* **96** 066402
[20] Allen J W and Martin R M 1982 *Phys. Rev. Lett.* **49** 1106
[21] Jarlborg T, Moroni E G and Grimvall G 1997 *Phys. Rev. B* **55** 1288
[22] Dudarev S L, Peng L M, Savrasov S Y and Zuo J M 2000 *Phys. Rev. B* **61** 2506
[23] Kresse G and Furthmuller J 1996 *Comput. Mater. Sci.* **6** 15
[24] Moruzzi V L, Janak J F and Schwarz K 1988 *Phys. Rev. B* **37** 790
[25] Wang Y, Ahuja R and Johansson B 2004 *Int. J. Quantum Chem.* **96** 501
[26] Voronov F F, Vereshchagin L F and Goncharova V A 1960 *Sov. Phys.—Dokl.* **135** 1280
[27] Wang Y 2000 *Phys. Rev. B* **61** R11863
[28] Koskenmaki D C and Gschneidner K A 1978 *Handbook on the Physics and Chemistry of the Rare Earths*
[29] Kutsar A R 1979 *Sov. Phys.—Dokl.* **24** 292
[30] Jayaraman A 1965 *Phys. Rev.* **137** A179
[31] Poniatovskii E G 1959 *Sov. Phys.—Dokl.* **3** 498
[32] Zachariasen W H and Ellinger F H 1977 *Acta Crystallogr.* A **33** 155
[33] Olsen J S, Gerward L, Benedict U and Itie J P 1985 *Physica* B+C **133** 129
[34] Stassis C, Loong C K, Kline G R, McMasters O D and Gschneidner K A 1978 *J. Appl. Phys.* **49** 2113
[35] van der Eb J W 2000 Cerium, one of nature's purest puzzles *PhD Thesis* University of Groningen
[36] Bastidet J P, Loriersf C, Massatf H and Coqblin B 1978 *Rare Earths and Actinides 1977* (Durham: Institute of Physics) p 66
[37] Ramakrishnan J and Kennedy G C 1980 *J. Appl. Phys.* **51** 2586
[38] Timusk T and Statt B 1999 *Rep. Prog. Phys.* **62** 61
[39] Norman M R, Pines D and Kallin C 2005 *Adv. Phys.* **54** 715
[40] Wikipedia 2009 http://en.wikipedia.org/wiki/Kondo_effect
[41] Kouwenhoven L and Glazman L 2001 *Phys. World* **14** 33
[42] Kondo J 1964 *Prog. Theor. Phys.* **32** 37

ed K A Gschneidner and L Eyring (Amsterdam: North-Holland) p 337